

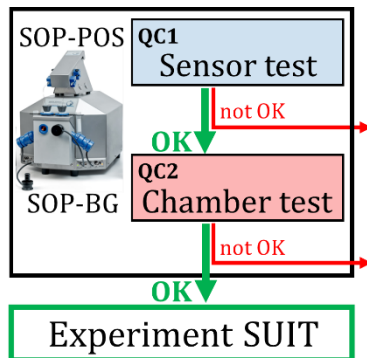
## Technical Communication

### Cite

Baglivo E, Cardoso LHD, Cecatto C, Gnaiger E (2022) Statistical analysis of instrumental reproducibility as internal quality control in high-resolution respirometry. MitoFit Preprints 2022.18.  
<https://doi.org/10.26124/mitofit:2022-0018.v1>

### Author contributions

EB and EG analyzed the data and wrote the manuscript; LHDC and CC collected data; all authors approved the final version of the manuscript.



### Conflicts of interest

EG is founder and CEO of Oroboros Instruments, Innsbruck, Austria.

Received 2022-05-05





Accepted 2022-05-05

Online 2022-05-05

### Keywords

high-resolution respirometry  
HRR;  
polarographic oxygen sensor POS;  
air calibration;  
instrumental background;  
reproducibility;  
limit of detection;  
internal quality control IQC;  
standard operating procedure SOP

# Statistical analysis of instrumental reproducibility as internal quality control in high-resolution respirometry

 Eleonora Baglivo,  Luiza HD Cardoso,  Cristiane Cecatto,  Erich Gnaiger\*

Oroboros Instruments, Innsbruck, Austria

\* Corresponding author: [erich.gnaiger@orooboros.at](mailto:erich.gnaiger@orooboros.at)

## Abstract

Evaluation of instrumental reproducibility is a primary component of quality control to quantify the precision and limit of detection of analytical procedures. A pre-analytical instrumental standard operating procedure (SOP) is implemented in high-resolution respirometry consisting of: (1) a daily SOP-POS for air calibration of the polarographic oxygen sensor (POS) in terms of oxygen concentration  $c_{O_2}$  [ $\mu\text{M}$ ]. This is part of the *sensor test* to evaluate POS performance; (2) a monthly SOP-BG starting with the SOP-POS followed by the *chamber test* quantifying the instrumental  $O_2$  background. The chamber test focuses on the slope  $dc_{O_2}/dt$  [ $\text{pmol}\cdot\text{s}^{-1}\cdot\text{mL}^{-1}$ ] to determine  $O_2$  consumption by the POS and  $O_2$  backdiffusion into the chamber as a function of  $c_{O_2}$  in the absence of sample. Finally, zero  $O_2$  calibration completes the sensor test.

We applied this SOP in a 3-year study using 48 Oroboros O2k chambers. Stability of air and zero  $O_2$  calibration signals was monitored throughout intervals up to 8 months without sensor service. Maximum drift over 1 to 3 days was  $0.06 \text{ pmol}\cdot\text{s}^{-1}\cdot\text{mL}^{-1}$ , without persistence over time since drift was  $<0.004 \text{ pmol}\cdot\text{s}^{-1}\cdot\text{mL}^{-1}$  for time intervals of one month, corresponding to a drift per day of 0.2 % of the signal at air saturation. Instrumental  $O_2$  background  $-dc_{O_2}/dt$  was stable within  $\pm 1 \text{ pmol}\cdot\text{s}^{-1}\cdot\text{mL}^{-1}$  when measured at monthly intervals.

**Data availability**

Original files are available  
Open Access at Zenodo  
repository:

[https://doi.org/10.26124/mitofit:  
2022-0018](https://doi.org/10.26124/mitofit:2022-0018)

**These results confirm the instrumental limit of detection of volume-specific O<sub>2</sub> flux at  $\pm 1$  pmol·s<sup>-1</sup>·mL<sup>-1</sup>. The instrumental SOP applied in the present study contributes to the generally applicable internal quality control management ensuring the unique reproducibility in high-resolution respirometry.**

## 1. Introduction

Quality control (QC) is essential to ensure experimental reproducibility. Proficiency testing (PT) aims at documenting and improving the technical performance of laboratories by independent quality assessments (Brookman, Mann 2021). PT targets the present lack of repeatability and reproducibility, and relies on implementation of PT schemes at substantial costs to accredited laboratories. Simpler strategies may be implemented into laboratory science as practical steps towards PT to achieve reproducibility (Amaral, Neves 2021). In our present study, we present an internal QC management tool (IQC) to evaluate the reproducibility of instrumental performance in high-resolution respirometry (HRR) using the Oroboros O2k (Oroboros Instruments, Innsbruck, Austria). We analyzed instrumental IQC tests performed in an experimental project conducted over three years (MiR05-Kit study). Instrumental testing represents IQC to assure the functioning of the instrument and to eliminate instrumental artifacts. In HRR the instrumental IQC tests – implemented as standard operating procedures (SOP) – are (1) daily oxygen *sensor tests* including air calibration in respiration medium, and (2) monthly *chamber tests* followed by a zero calibration of the polarographic oxygen sensor (POS; Gnaiger 2001; 2008; Doerrier et al 2018). The stability of two-point calibrations (air and zero) and the response time of the POS reflect the major performance characteristics of the sensor. The instrumental O<sub>2</sub> background flux in the absence of sample represents the chamber test to evaluate O<sub>2</sub> consumption independent of the sample and O<sub>2</sub> backdiffusion into the chamber as a function of O<sub>2</sub> concentration.

Diffusion of oxygen between an experimental chamber and its surroundings is zero in an ideal closed system. A closed system is defined in physical chemistry by system boundaries which prevent the exchange of matter – including oxygen – but allow for the exchange of energy, specifically exchange of heat under isothermal conditions in a thermostat. In reality, however, ‘closed’ experimental chambers may not perform as ideal closed systems. The aqueous phase (respiration medium) containing the sample within the chamber is separated by an oxygen-permeable membrane from the electrolyte, cathode, and anode of the POS. The electrochemical detection of *c*<sub>02</sub> in the respiration medium by the POS is based on O<sub>2</sub> consumption at the cathode, and as such, the experimental system is open for O<sub>2</sub> diffusion across the POS-membrane to the cathode. By design, the corresponding O<sub>2</sub> consumption by the POS is part of the instrumental O<sub>2</sub> background flux. In contrast, any unwarranted leaks at the sealings of the closed chamber cause inappropriate O<sub>2</sub> backdiffusion into the chamber at declining experimental *c*<sub>02</sub>, resulting in artifacts of respirometric measurements, if not corrected for. The SOPs

applied in the present study and the statistical analyses of instrumental tests provide the basis for evaluating the limit of detection and uncertainty in the measurement of volume-specific respiratory flux by HRR. Successful implementation of these IQC procedures into any experimental project on HRR and reporting of IQC results contribute to reproducibility and the quality of research in mitochondrial physiology.

## 2. Materials and methods

### 2.1. Chemicals

Mitochondrial respiration medium – MiR05 (Gnaiger et al 2000): 0.5 mM EGTA, 3 mM MgCl<sub>2</sub>·6H<sub>2</sub>O, 60 mM lactobionic acid, 20 mM taurine, 10 mM KH<sub>2</sub>PO<sub>4</sub>, 20 mM 2-[4-(2-hydroxyethyl)piperazin-1-yl]ethanesulfonic acid HEPES, 110 mM sucrose, 1 g/L BSA; pH 7.1 (KOH); prepared using MiR05-Kit (Oroboros Instruments, Austria, ID: 60101-01) and BSA (bovine serum albumin, fraction V, Sigma-Aldrich, cat. N° A6003).

Chemicals for background test (MiPNet14.06 2020): Dithionite solution was prepared using O<sub>2</sub>-Zero Powder (Oroboros Instruments, ID: 26600-01): 0.017 g Na<sub>2</sub>S<sub>2</sub>O<sub>4</sub> is dissolved in 10 mL total volume phosphate buffer to obtain 10 mM dithionite solution. Phosphate buffer: 47 mM K<sub>2</sub>HPO<sub>4</sub> (cat. N° P8281) and 3.3 mM KH<sub>2</sub>PO<sub>4</sub> (cat. N° P5655) from Sigma-Aldrich. All solutions were prepared with deionized ultra-pure H<sub>2</sub>O (Ultra ClearTMTP UV UF TM, Evoqua Water Technologies GmbH).

### 2.2. Open and closed chamber

2.1 to 2.5 mL MiR05 (pre-warmed to approximately 40 °C) were filled into the O2k-chamber containing the rotating stirrer. The stopper (calibrated for a chamber volume of 2 mL) was inserted completely, excess medium was siphoned off the stopper receptacle, and the stopper was partially pulled up into a position defined by the Stopper-Spacer (Oroboros Instruments, Austria; ID: 24420-01). This is defined as ‘open chamber’, in contrast to the ‘closed chamber’, referring to the condition of a fully inserted stopper with 2.0 mL aqueous medium and no gas phase.

### 2.3. Settings of the TIP2k

200 µL-TIP2k syringes were filled with freshly prepared dithionite solution and mounted on the TIP2k (Oroboros Instruments, Austria; ID: 11100-03). To soak up excess liquid, TIP2k-Filter papers (Oroboros Instruments, Austria; ID: 31320-01) were placed on the Stoppers. TIP2k needles were inserted into the O2k chambers through the stopper, avoiding contact with the stirrer bar in the chamber by adjusting the TIP2k-Needle Spacers. The TIP2k setup was loaded in the software DatLab 7.4 and the TIP2k program was started for automatic control of dithionite injections at 20 min time intervals. After a delay of 20 min, the first dithionite injection was programmed to 0.25 µL/s, stopping at an O<sub>2</sub> concentration  $c_{O_2} < 100$  µM. The second dithionite injection was programmed at 0.125 µL/s, stopping at  $c_{O_2} < 50$  µM; the third injection at 0.05 µL/s stopping at  $c_{O_2} < 23$  µM; and finally, 50 µL dithionite was titrated in 1 s to reduce  $c_{O_2}$  to 0 µM.

## 2.4. High-resolution respirometry

O<sub>2</sub> flux was measured in the Oroboros O2k. The O2k-chambers were calibrated at experimental volumes of 2 mL and at experimental temperature of 37 °C (stability ±0.002 °C). The medium was continuously stirred with a polyether ether ketone (PEEK)-coated magnetic stirrer bar at 750 rpm for optimum signal stability of the POS and mixing of the suspended sample and dissolved substances. DatLab 7.4 was used for data acquisition and analysis. The O<sub>2</sub> signal of POS was recorded at 2 s time intervals and volume-specific oxygen flux  $J_{V,O_2}$  [pmol·s<sup>-1</sup>·mL<sup>-1</sup>] was calculated real-time as the negative time derivative of the O<sub>2</sub> concentration,  $-dc_{O_2}/dt$ , and plotted continuously (Figures 1 and 2b).

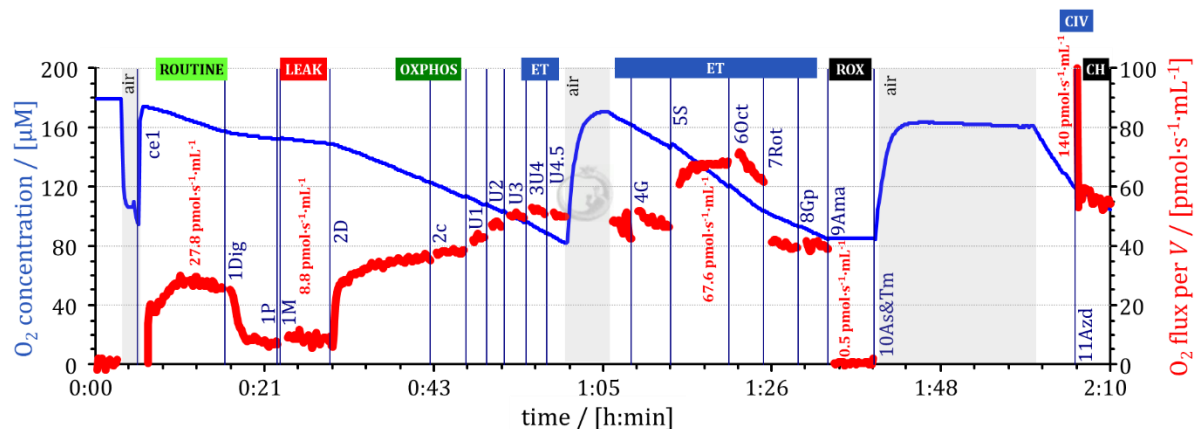


**Figure 1. Experimental SUIT protocol.** Trace of oxygen concentration (blue line) and volume-specific oxygen flux (red line; corrected for instrumental background O<sub>2</sub> flux) in the protocol SUIT-001 over a period of 2 h and 10 min. Oxygen concentration was kept above 80 μM by intermittent reoxygenations (open chamber, gray shade). Horizontal bars: respiratory states (selected corresponding rates are shown by numbers); vertical lines: events in sequential titrations. **ce1**: addition of HEK 293T cryopreserved cells (10<sup>6</sup> x·mL<sup>-1</sup>) while the stirrer was stopped and the stopper intermittently removed, with subsequent ROUTINE respiration of living cells. **1Dig**: digitonin (10 μg·mL<sup>-1</sup>) to permeabilize the plasma membrane. **1P** & **1M**: pyruvate (5 mM) & malate (2 mM), inducing LEAK respiration. **2D**: ADP (2.5 mM) to kinetically saturate OXPPOS capacity. **2c**: cytochrome *c* (10 μM) to test the integrity of the mitochondrial outer membrane. **U1** to **U4.5**: titrations of uncoupler (CCCP; numerals indicate the concentration [μM]), to obtain maximum oxygen flux (3U4) as a measure of electron transfer (ET) capacity. **air**: reoxygenation in the open chamber, when O<sub>2</sub> flux is not measured. **4G**: glutamate (10 mM). **5S**: succinate (50 mM). **6Oct**: octanoylcarnitine (0.5 mM). **7Rot**: rotenone (0.5 μM). **8Gp**: glycerophosphate (10 mM). **9Ama**: antimycin A (2.5 μM), inhibiting flux to residual oxygen consumption ROX. **10As&Tm**: ascorbate (2 mM) & TMPD (0.5 mM). After a 20 min period with an open chamber (air), As&Tm-stimulated CIV activity includes chemical autooxidation (CH) measured after inhibiting Complex IV by **11Azd**: azide (200 mM). Experiment 2021-11-16 P1-04 (QC data repository).

A representative trace using the substrate-uncoupler-inhibitor-titration SUIT-001 protocol (Figure 1) with HEK 293T cryopreserved cells (Doerrier et al 2018; Gnaiger 2020) illustrates the experimental protocol applied in a 3-year study on the stability of

the MiR05-Kit (in preparation). Experimental oxygen concentrations ranged from air saturation (180  $\mu\text{M}$ ) to a minimum of 30  $\mu\text{M}$  in the entire study. To maintain this oxygen regime, several reoxygenations were required in the time course of experiments up to 2 h 30 min. Volume-specific  $\text{O}_2$  flux  $J_{V,\text{O}_2}$  in various respiratory states is indicated in [Figure 1](#), reaching a maximum of 140  $\text{pmol}\cdot\text{s}^{-1}\cdot\text{mL}^{-1}$ . Antimycin A-inhibited residual oxygen consumption reached the limit of detection specified at 1  $\text{pmol}\cdot\text{s}^{-1}\cdot\text{mL}^{-1}$  (MiPNet18.10 2019). The MiR05-Kit study included 16 O2k-Series H chambers in a one-day experiment (2019-12); 14 O2k-Series H chambers in a two-days experiment (3 days apart; 2020-11); and 16 O2k-Series I chambers in a two-days experiment (1 day apart; 2021-11).

## 2.5. Oxygen sensor calibration and instrumental $\text{O}_2$ background test

The oxygen sensor test includes two calibration steps and additional tools for quality control of (1) response time, (2) long-term stability, and (3) noise of the sensor signal ([Figure 2](#)). The sensor test is performed under experimental conditions in the absence of sample. It starts in an 'open chamber' when the liquid phase – containing MiR05 in the present study – was allowed to equilibrate with air in the gas phase at an average barometric pressure of 94.9 kPa (Innsbruck; 575 m altitude), partial  $\text{O}_2$  pressure of 18.6 kPa, and equilibrium  $\text{O}_2$  concentration in MiR05 of 180  $\mu\text{M}$ . First, the stirrer test was performed to evaluate the dynamic response behavior of the POS. The stirring is switched off for 30 s and after switching on the stirrer rotation, a rapid and mono-exponential increase of the oxygen signal indicated a proper response time of the POS ([Figure 2c](#)). The oxygen signal reached stability after equilibration of the aqueous medium with air in the gas phase of the open chamber. The air calibration mark R1 is set on the plot of the oxygen signal at air saturation (MiPNet06.03 2022).

After closing the chamber, the focus is switched from the sensor signal to the time derivative of the oxygen signal in the closed chamber, as the initial step of the chamber test, still in the absence of sample. The chamber was closed by fully inserting the stopper to extrude the gas phase, which may cause a disturbance of the oxygen signal and a short fluctuation of the slope ([Figure 2b](#)). Subsequently, the needle of the TIP2k was inserted and the TIP2k program of DatLab started with a 20 min delay, during which the oxygen consumption by the POS was recorded. The mark  $J^{\circ}_1$  was set on the plot 'negative slope'. Then the TIP2k program controls injections of dithionite solution at 20 min time intervals to reduce oxygen concentration to defined levels and allow for stabilization of the slope. Marks  $J^{\circ}_2$ ,  $J^{\circ}_3$ , and  $J^{\circ}_4$  were set at the end of each interval when the slope was nearly constant, to calculate the median slope at the corresponding  $\text{O}_2$  concentration for each mark.  $\text{O}_2$  consumption by the POS is gradually compensated for by  $\text{O}_2$  backdiffusion into the chamber at declining  $\text{O}_2$  concentrations, eventually leading to a predominance of  $\text{O}_2$  backdiffusion and a negative value of the negative slope.

At this point, the chamber test is concluded, and the focus is switched again to the oxygen signal. Sensor calibration is finalized by the TIP2k program, this time keeping the chamber closed ([Figure 2a](#)). An excess concentration of dithionite was titrated into the closed chamber, to completely reduce the oxygen, and the zero-oxygen calibration mark R0 is then set on the plot of the oxygen signal ([Figure 2d](#)).



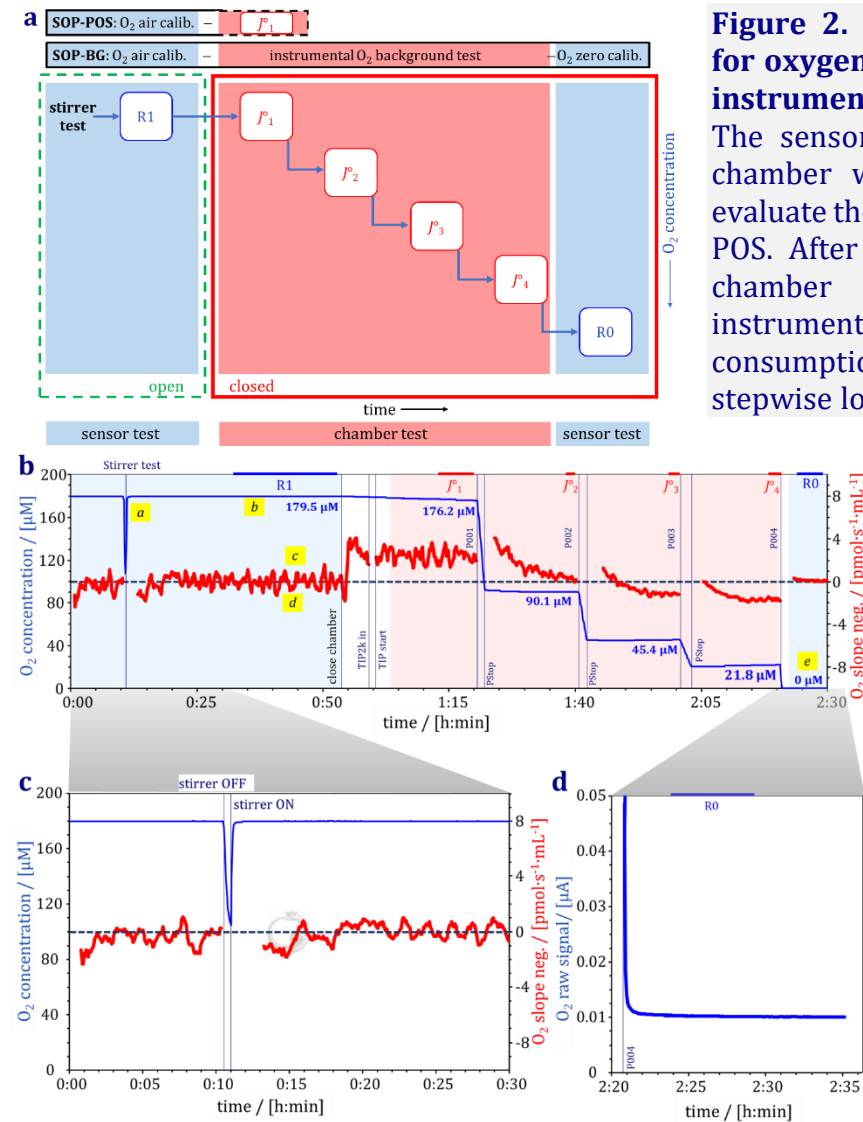


**Figure 2. Instrumental protocols for oxygen sensor calibration and instrumental O<sub>2</sub> background test.**

The sensor test starts in an open chamber with the stirrer test, to evaluate the dynamic response of the POS. After air calibration (R1) the chamber is closed and the instrumental background O<sub>2</sub> consumption  $J^{\circ}_1$  to  $J^{\circ}_4$  is measured at stepwise lowered O<sub>2</sub> concentrations.

Finally, zero oxygen calibration R0 is part of the sensor test. **(a)** Scheme of O2k instrumental SOPs. SOP-POS: O<sub>2</sub> air calibration protocol, possibly continued by measurement of  $J^{\circ}_1$ . SOP-BG: instrumental O<sub>2</sub> background protocol, combined sensor test and chamber test. **(b)** Representative traces of SOP-BG. Calibrated oxygen concentration (blue line [μM]) and negative slope (red line [pmol·s<sup>-1</sup>·mL<sup>-1</sup>]).

Vertical lines represent events (P001 to P004: automatic TIP2k titrations), horizontal bars represent marks. Blue shaded sections indicate the sensor test. In the first section air calibration is performed in the open chamber including the stirrer test (panel c). When stability of the oxygen signal is reached (red line; zero slope), the air calibration signal R1 is obtained from the first mark set on the oxygen concentration plot. The final section of the sensor test represents zero oxygen calibration with mark R0 on the oxygen concentration plot (panel d), obtained in the closed chamber after titration of an excess concentration of dithionite which depletes oxygen completely. The red shaded section indicates the period of chamber test, when the chamber is closed and the TIP2k program started. During the first 20 min delay, O<sub>2</sub> consumption by the POS is recorded near air saturation (mark  $J^{\circ}_1$  on the red plot at 176.2 μM). The oxygen concentration is stepwise reduced to defined levels by the TIP2k program by injecting dithionite solution at 20 min time intervals. Marks  $J^{\circ}_2$ ,  $J^{\circ}_3$ , and  $J^{\circ}_4$  were set at O<sub>2</sub> concentration of 90.05, 45.4, and 21.8 μM, respectively. The slope is not shown during the phases of dithionite-induced decline of oxygen concentration. The letters (a to d) refer to

the discussion. **(c)** Zoom into the section of the stirrer test. Stirrer rotation of stirrers of both chambers is switched off for 30 s. After switching on the stirrer rotation, the increase of the oxygen signal should be rapid and monoexponential. **(d)** Zoom into the oxygen signal at zero calibration  $R_0$ , reached after complete reduction of the oxygen in the closed chamber.

Data was recorded at 2-s intervals. 60 data points were selected for the marks, but even 30 points were sufficient for obtaining reproducible results.

## 2.6. Sensor service

Service of the polarographic oxygen sensor (MiPNet19.18B 2021) was performed at intervals of a few months or more than one year to maintain high time resolution, low noise, and signal stability of the sensor. This includes cleaning of anode and cathode, exchange of electrolyte, and membrane mounting. The sensor test helps to determine if a sensor service is required.

## 2.7. Statistics

The raw signal and slope of the oxygen concentration in marked sections of the plots were computed by DatLab 7.4 as the medians of data points measured or calculated, respectively, across the marked sections.

In regressions between variables in  $X$  and  $Y$  with identical errors of measurement – see regressions between first and second calibrations (Figure 3a) – the ordinate  $Y/X$  slope  $b_Y$  is underestimated compared to the inverted  $X/Y$  slope  $b_X$  calculated from the abscissal  $X/Y$  slope  $\beta_X$ . The coefficient of determination  $r^2$  is independent of inversion of the axes. At high  $r^2$ , mean inverted regression lines were calculated by inverted regression analysis using Excel (Gnaiger 2021). To minimize the residuals of both variables,  $Y$  and  $X$ , slopes  $b_Y$  and  $\beta_X$  and intercepts  $a_Y$  and  $a_X$  are calculated for the  $Y/X$  and  $X/Y$  inverted linear regressions, respectively. The mean slope  $\bar{b} = (b_Y + b_X)/2$  and mean intercept  $\bar{a} = (a_X + a_Y)/2$  are used, where  $b_X = 1/\beta_X$  and  $a_X = -a_Y/\beta_X$  (Gnaiger 2021). At  $r^2$  close to zero,  $b_Y$  is nearly zero leading to a horizontal line, whereas  $b_X$  corresponds to a vertical line. In this case, mean slopes and intercepts are meaningless, and the inverted regression lines are shown separately to visualize the lack of a correlation. In regressions between  $Y = -dcO_2/dt$  and  $X = cO_2$ , variability in  $X$  is small compared to variability in  $Y$ , hence ordinate regression analysis is appropriate (Figure 6).

## 3. Results

### 3.1. Oxygen calibration

The limit of detection of  $J_{V,O_2}$  depends on accurate  $O_2$  calibration of the polarographic oxygen sensor, signal stability, and corrections of the slope over time. A functional POS must provide a sensitive and linear response to partial oxygen pressure with stable

sensitivity. Sensitivity is the raw signal [ $\mu\text{A}$ ] divided by oxygen concentration [ $\mu\text{M}$ ]. In addition, low noise and fast response of the oxygen signal to changes in oxygen concentration are required for adequate time resolution (Figure 2).

In 30 different POS, zero-corrected air calibration signals, R1-R0, ranged from 1.8 to 2.3  $\mu\text{A}$  (Figure 3a). The stability of the air calibration signal R1 of each sensor was evaluated over time intervals of 1 to 3 days, applying the instrumental protocol SOP-POS (Figure 2a). The deviation between calibrations R1#1 and R1#2 indicates a drift per day of up to 1.0 % (or 2.7 % including the single data point with maximal deviation) for an  $\text{O}_2$  concentration at air saturation of 180  $\mu\text{M}$ . These values correspond to a slope of 0.02  $\text{nM}\cdot\text{s}^{-1}$  or 0.02  $\text{pmol}\cdot\text{s}^{-1}\cdot\text{mL}^{-1}$  (0.06  $\text{pmol}\cdot\text{s}^{-1}\cdot\text{mL}^{-1}$  including the single data point). This low drift per day supports the standard R1 calibration procedure performed daily before the experiments (R1#1), without further consideration of the following R1#2.

The stability of calibration signals was evaluated over time intervals of 27 to 38 days in applications of the instrumental  $\text{O}_2$  background protocol SOP-BG (Figure 3b). R1-R0 of 46 different POS ranged from 1.7 to 2.4  $\mu\text{A}$  with a maximal deviation between two calibration points corresponding to a drift per day of 0.16 %, 0.21 %, and 0.10 % or 0.003, 0.004, and 0.002  $\text{pmol}\cdot\text{s}^{-1}\cdot\text{mL}^{-1}$  for 2019, 2020 and 2021, respectively (Figures 3d to f). Comparing these values with the maximal slope of 0.02 to 0.06  $\text{pmol}\cdot\text{s}^{-1}\cdot\text{mL}^{-1}$  calculated between calibrations separated by 1 to 3 days (Figure 3a), confirms that the maximal drift does not persist over the month. As expected, R1-R0 values show better stability when calibration R1#1 and R1#2 are separated by smaller time intervals, justifying again the daily R1 calibration.

When performing SOP-BG, signal R0 is optionally calibrated as the final step. R0 ranged from 0.00 to 0.05  $\mu\text{A}$  (Figure 3c; to 0.10  $\mu\text{A}$  including the single maximum data point out of range). The maximal deviation between two R0 calibration points was 0.02  $\mu\text{A}$  (0.08  $\mu\text{A}$  including the maximum data point), indicating stability of R0 over a time interval of a month or longer.  $\text{R0}/(\text{R1}-\text{R0})$  was maximally 2.2 % (5 % including the maximum data point), quantifying the magnitude of R0 on R1-R0 (Data repository QC\_R1-R0). These results validate the monthly performance of zero oxygen calibration. For the record, once a spurious R0 value (5.7 % of R1) was obtained in calibration R0#2 in O2k P7A in 2020. The calibration was repeated immediately without POS service, and the new R0#3 was accepted (1.5 % of R1) since it was consistent with calibration R0#1.

There was no correlation between the calibration values R1-R0 in chamber A and chamber B of the same O2k, measured simultaneously, confirming that each chamber can be considered independently in the experimental design (Figure 4).

Experiments in the MiR05-Kit study involving 40 POS were timed within intervals of 3 to 8 months without sensor service, during which air and zero calibrations R1 and R0 were performed routinely in various O2k applications. The relative change of R1 was generally  $<\pm 0.10$  over all time intervals (Figure 5; Data repository QC\_Change of R1). R0 was maximally 1.8 % (2019 and 2020) and 1.9 % (2021) of R1, with a single value reaching 2.2 % (Data repository QC\_R0 over R1).



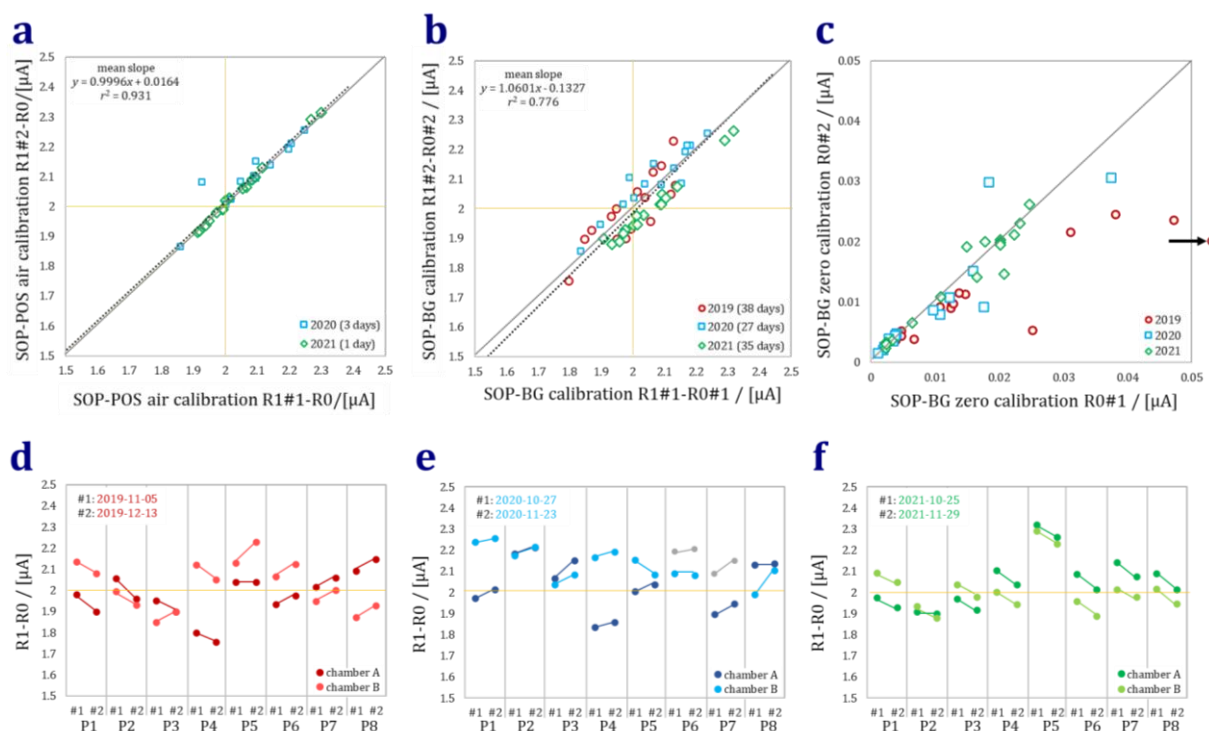


**Figure 3. Stability of calibration signals of oxygen sensors from 1 to 3 days and 27 to 38 days.** (a) R0-corrected air calibration signals R1-R0 [ $\mu\text{A}$ ] of 30 oxygen sensors with R1#1 measured in SOP-POS before each experiment (Figure 1) and R1#2 measured 3 or 1 days later (2020 and 2021, respectively). Full line: theoretical line of correspondence if calibrations R1#1 and R1#2 are identical; dotted line: mean inverted regression line, indicating a proportional relationship ( $r^2= 0.93$ ); horizontal and vertical lines with intercept at 2/2: default R1 setting. Experiments were restricted to a single day in 2019 and are, therefore, not applicable for this analysis. (b) Stability of R0-corrected air calibration signals of 46 sensor with R1 and R0 measured in consecutive applications of SOP-BG (calibrations #1 and #2; 38, 27, and 35 days apart in 2019, 2020 and 2021, respectively). Horizontal and vertical lines with intercept at 2/2: default R1 setting; full line: theoretical line of correspondence if calibrations #1 and #2 are identical; dotted line: mean inverted regression line, indicating a proportional relationship ( $r^2= 0.78$ ). (c) Stability of zero oxygen calibration R0 of 46 oxygen sensors between calibrations R0#1 and R0#2 in SOP-BG (panel b). The arrow indicates a single data point out of range at 0.10/0.02 (P5A in 2019). An especially good proportionality is shown in data from 2021 ( $r^2= 0.93$ ), while the ones from 2019 are more scattered ( $r^2= 0.80$ ). (d) to (f) R1-R0 signals, measured in SOP-BG (panel b), are shown for 16, 14, and 16 individual sensors (2019, 2020, and 2021, respectively; chambers P6A and P7B were not used in the MiR05-Kit study). Vertical lines separate different O2k. Dots with the same color and connected by lines represent values of calibrations #1 and #2 for the same sensor.

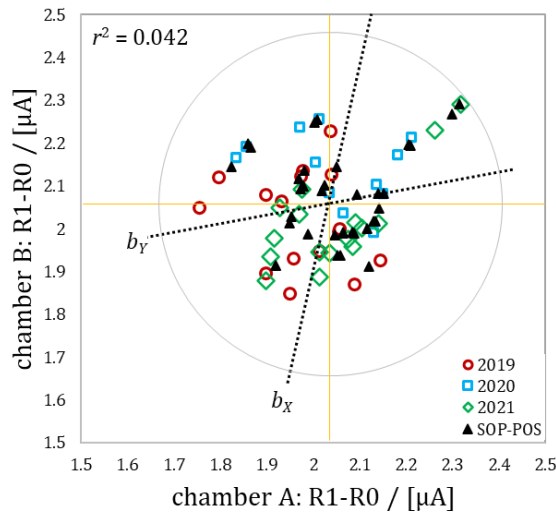


**Figure 4. No correlation between calibration values in chambers A and B of the same O2k, measured simultaneously, indicating that each chamber can be considered independently in the experimental design.** Dotted lines: ordinate  $b_Y$  and abscissal  $b_X$  regression lines, with a cross-over point of  $X^*= 2.03 \mu\text{A}$  and  $Y^*= 2.06 \mu\text{A}$  (vertical and horizontal lines), compared to the medians of  $2.04$  and  $2.05 \mu\text{A}$ , close to the default value of  $2 \mu\text{A}$ . Black symbols represent calibrations signals with a time interval up to 3 days (SOP-POS). The circle, centered at the cross-over point, indicates the lack of interdependence with circular data distribution.

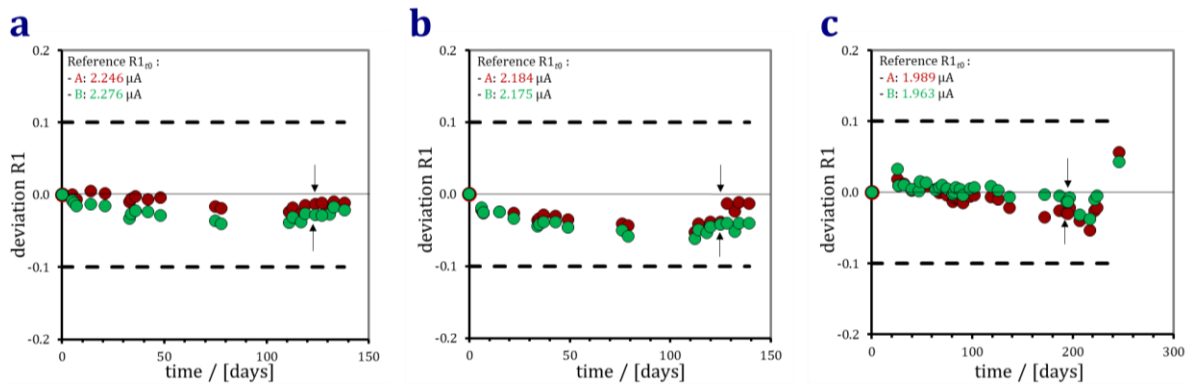


**Figure 5. Stability of air calibration signals of oxygen sensors over time.** Examples of 3 O2k at air saturation over 6 months (a, b; P2 and P3 in 2020) and 8 months (c; P2 in 2021). Red dots: chamber A; green dots: chamber B. The first R1 value after sensor service is shown as reference  $R1_{t_0}$  in each figure. The relative deviation of  $R1_t$  over time is the fraction  $(R1_t - R1_{t_0})/R1_{t_0}$ . The relative change was generally less than  $\pm 0.10$ , indicating that R1 values were stable over time. The calibration points of the MiR05-Kit experiment (Figure 1) are indicated by arrows.

The presented results point out the stability of oxygen calibration signals R1 and R0 for time intervals of (1) few days, (2) about one month, and (3) up to 8 months, and justify the applied SOP for air and zero calibrations (Supplement Figure S1b).

### 3.2. Instrumental O<sub>2</sub> background test

The O<sub>2</sub> background test (BG) is performed as a chamber test to (1) exclude any microbial contamination of the respiration medium, (2) quantify the oxygen consumption by the POS close to air saturation in mark  $J^{\circ}_1$  (O<sub>2</sub> concentration dropped from 180 to 176  $\mu\text{M}$ ), and (3) evaluate the deviation from an ideally closed chamber due to O<sub>2</sub> backdiffusion in sections marked as  $J^{\circ}_2$  to  $J^{\circ}_4$ .

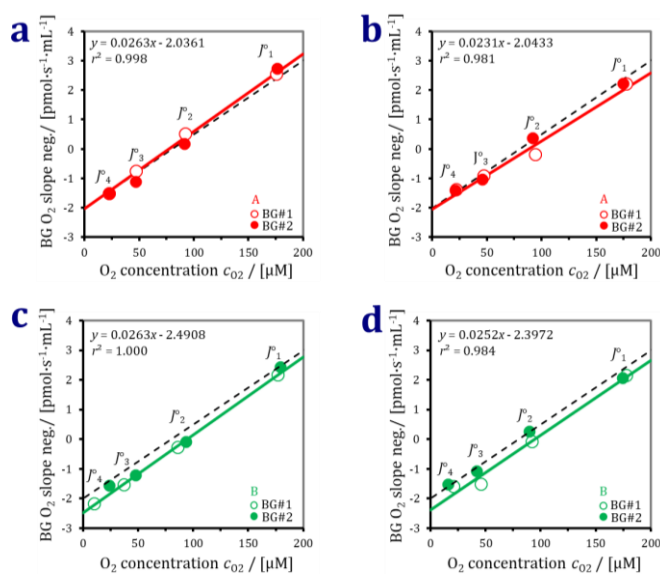


**Figure 6. Stability of O<sub>2</sub> background test.** Representative examples of 4 O<sub>2</sub>k chambers for background (BG) tests separated by 27 days (**a**: P8A, **c**: P8B; in 2020) and 35 days (**b**: P3A, **d**: P3B; in 2021). Negative BG O<sub>2</sub> slope plotted as a function of oxygen concentration for the four background marks (J<sub>1</sub> to J<sub>4</sub>). Open circles: BG#1, with corresponding regression line (full line); closed circles: BG#2, showing the deviation from BG#1 regression line. Dashed lines: default intercept  $a^\circ = -2.0 \text{ pmol}\cdot\text{s}^{-1}\cdot\text{mL}^{-1}$  and slope  $b^\circ = 0.025$ .

Linear regressions were calculated to express the dependence of the negative slope of the oxygen signal on O<sub>2</sub> concentration c<sub>O2</sub>. For BG#1 the intercept  $a^\circ$  at zero c<sub>O2</sub> ranged from -1.2 to -3.5 pmol·s<sup>-1</sup>·mL<sup>-1</sup> and the slope  $b^\circ$  from 0.021 and 0.035 in 40 different O<sub>2</sub>k chambers (Data repository QC\_Background). Representative analyses are shown in Figure 6.

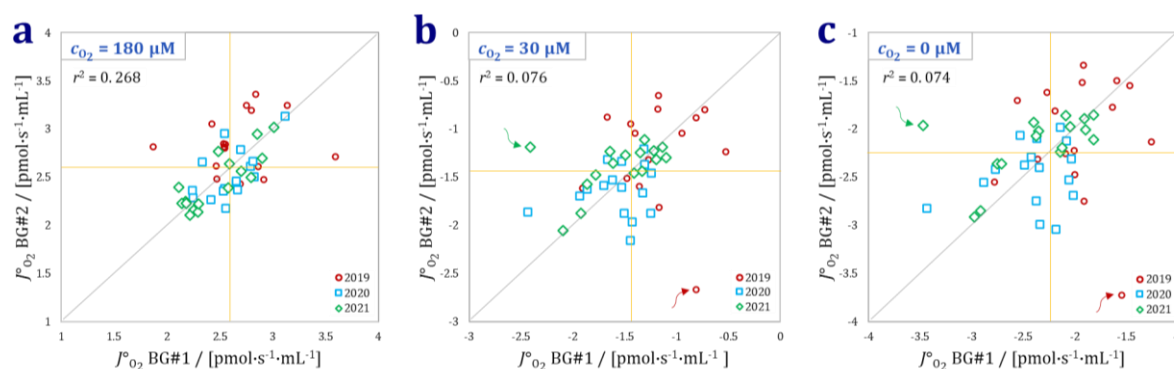


**Figure 7. Stability of instrumental background O<sub>2</sub> flux at different O<sub>2</sub> concentrations up to 38 days.** Instrumental background oxygen flux J<sub>O<sub>2</sub></sub> of 48 O<sub>2</sub>k chambers at O<sub>2</sub> concentrations 180 μM, 30 μM, and 0 μM in (**a**), (**b**), and (**c**), respectively. Full line: theoretical line of correspondence if J<sub>O<sub>2</sub></sub> of BG#1 and BG#2 are identical. Horizontal and vertical lines show the average intercepts of J<sub>O<sub>2</sub></sub> for each c<sub>O2</sub>. Chamber 4B in 2019 indicated increased O<sub>2</sub> backdiffusion in BG#2 compared to BG#1 (red arrows). Chamber 8A in 2021 had higher O<sub>2</sub> backdiffusion in BG#1 compared to BG#2 (green arrows in panels b and c).

The stability of background corrections was evaluated for a time interval up to 38 days after BG#1, repeating the BG test in BG#2 as an ‘experimental mimetic’ without sample. Using the regression parameters, the instrumental background O<sub>2</sub> flux J<sub>O<sub>2</sub></sub> was calculated at air saturation ( $2.6 \pm 0.3 \text{ pmol}\cdot\text{s}^{-1}\cdot\text{mL}^{-1}$  at 180 μM), at the lowest c<sub>O2</sub> observed

in the MiR05 study ( $-1.4 \pm 0.4 \text{ pmol}\cdot\text{s}^{-1}\cdot\text{mL}^{-1}$  at  $30 \mu\text{M}$ ), and at the intercept for zero oxygen ( $-2.2 \pm 0.5 \text{ pmol}\cdot\text{s}^{-1}\cdot\text{mL}^{-1}$  at  $0 \mu\text{M}$ ; Figure 7).

The difference  $\Delta J^{\circ}\text{O}_2$  between  $J^{\circ}\text{O}_2$  of BG#2 and BG#1 at each  $c_{\text{O}_2}$  was in the range  $\pm 1 \text{ pmol}\cdot\text{s}^{-1}\cdot\text{mL}^{-1}$ , with two exceptions (chamber 4B from 2019 and 8A from 2021; Figure 8). The absolute  $\Delta J^{\circ}\text{O}_2$  was maximally 0.9, 0.8 (or 1.9 with the data point out of range), and 0.9 (or 2.2 with the data point out of range)  $\text{pmol}\cdot\text{s}^{-1}\cdot\text{mL}^{-1}$  for 180, 30, and  $0 \mu\text{M}$ , respectively.

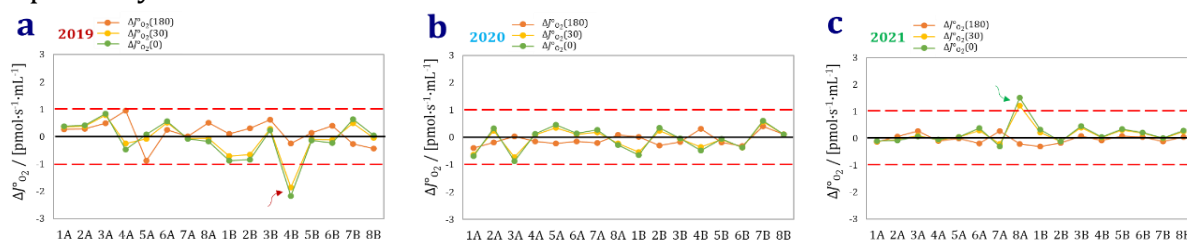


**Figure 8. Stability of  $J^{\circ}\text{O}_2$  difference at different  $\text{O}_2$  concentrations up to 38 days.** The difference  $\Delta J^{\circ}\text{O}_2$ , evaluated as  $J^{\circ}\text{O}_2(\text{BG}\#2) - J^{\circ}\text{O}_2(\text{BG}\#1)$ , of 48 O2k chambers at 180, 30, and  $0 \mu\text{M}$  is shown for 2019 (a), 2020 (b), and 2021 (c).  $\Delta J^{\circ}\text{O}_2$  values were evaluated for time intervals of 38, 27, and 35 days for 2019, 2020, and 2021, respectively. Dashed lines: limit of detection ( $\pm 1 \text{ pmol}\cdot\text{s}^{-1}\cdot\text{mL}^{-1}$ ), indicating the residuals after background correction. 3 % of the data points exceeded the limit of detection for  $\Delta J^{\circ}\text{O}_2(30)$  and  $\Delta J^{\circ}\text{O}_2(0)$ , in the same chambers as in Figure 7 identified by red and green arrows.

In summary, these results suggest that the background correction performed with BG#1 is sufficient for a one-month period to obtain a limit of detection of  $J_{V,\text{O}_2}$  of  $\pm 1 \text{ pmol}\cdot\text{s}^{-1}\cdot\text{mL}^{-1}$ . Averaging BG#1 and BG#2 might improve the results further, but this option turned out to be unnecessary.

## 4. Discussion

Instrumental testing provides quality control to evaluate instrumental performance. The most comprehensive instrumental test in HRR is the SOP-BG (Figure 9). It includes both the sensor and chamber test and is obligatory before proceeding with experiments. The SOP-BG, however, is time-consuming and therefore requires an economic planning of the frequency of conducting the entire procedure. The sensor test represents the first quality control QC1, to check the functional characteristics of the POS and to decide on the necessity of performing a sensor service. The individual criteria of the sensor test are summarized in Figure 2b. (a) A rapid and mono-exponential response of the oxygen signal in the stirrer test (Figure 2c) is of primary importance in kinetic studies (Gnaiger 2001). The accurate response time is less important in analyses of respiratory states at constant respiration, such as in SUIT protocols (Gnaiger et al 2020), except if the sensor response is as slow as to delay the effect of titrations on the respiratory rate. (b) The raw signal R1 was in a narrow range of 1.8 to 2.4  $\mu\text{A}$  in different sensors. R1 was stable in every sensor over several months. (c) Signal stability was expressed as the time derivative  $-dc_{\text{O}_2}/dt$  across the section of R1 marks (medians). Stability was within  $\pm 1 \text{ pmol}\cdot\text{s}^{-1}\cdot\text{mL}^{-1}$ , with a maximal absolute instability of 0.9

$\text{pmol}\cdot\text{s}^{-1}\cdot\text{mL}^{-1}$  (Figure S1a). (d) Noise of the signal was evaluated as the standard deviation (SD) of the data points in the plots of the  $\text{O}_2$  slope. SD over a time interval of about 5 min was typically  $0.6 \text{ pmol}\cdot\text{s}^{-1}\cdot\text{mL}^{-1}$  (Figure 2b). Noise is related to the response time since a slower response acts effectively as a filter and implicates lower noise. (e) Zero calibration signals  $R_0$  were  $<2\%$  of  $R_1$ , with a single value reaching  $2.2\%$ .

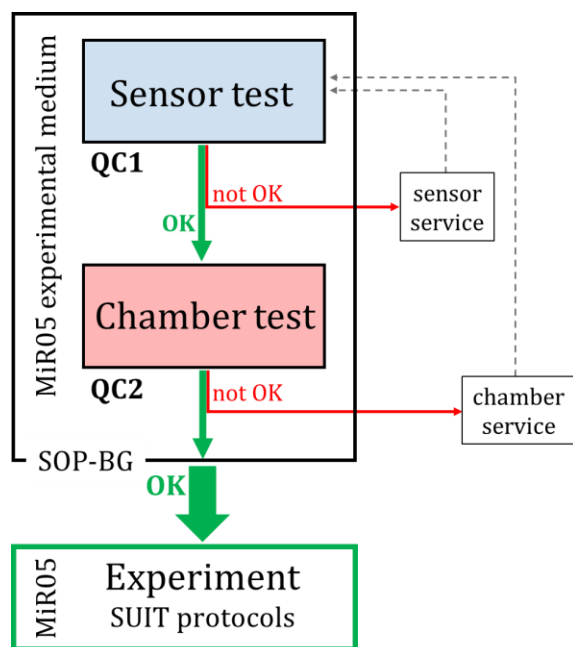


**Figure 9. Quality control scheme for evaluation of instrumental performance by application of SOP-BG.** QC1: sensor test, to check characteristics of the POS; if it fails, a sensor service is required. QC2: chamber test to ensure the optimal functional state of the  $\text{O}_2\text{k}$  chamber; if it fails, a chamber service is required. Statistical analysis of results in QC1 and QC2 provides the instrumental reference for interpreting the uncertainty of experimental results.

Even if QC1 indicates a proper function of the oxygen sensor, the chamber test is required as QC2, since it reflects the characteristics of the respirometric chamber and the incubation medium. Any microbial contamination can be detected as an elevated

instrumental background  $\text{O}_2$  consumption  $J^{\circ}_1$  which is measured close to air saturation. This step is included in the SOP-POS for daily control and in the chamber test of SOP-BG followed by controlled variations of  $c_{\text{O}_2}$  levels in the absence of sample. The range of  $c_{\text{O}_2}$  selected in the chamber test should match the experimental oxygen regime (Pesta, Gnaiger 2012). At low oxygen levels, any leak of the chamber is detected as an increased  $\text{O}_2$  backdiffusion. A proper outcome of both QC1 and QC2 minimizes instrumental errors and allows for evaluation of their effects on experimental results.

The limit of detection of  $\text{O}_2$  flux is reported only for HRR (Gnaiger 2001). Several comparisons of respiratory platforms provide narratives on the different experimental approaches without statistical evaluation of their performance relative to HRR (Horan et al 2012; Zhang et al 2012; Perry et al 2013). In experiments using a multiwell platform, instrumental background data are not routinely reported (Seahorse XF Analyzer; Yépez et al 2018). To compare instrumental resolution in the Seahorse XF Analyzer and Oroboros  $\text{O}_2\text{k}$ , Zdrzilova et al (2022) evaluated residual oxygen consumption measured in both platforms after inhibiting mitochondrial electron transfer by rotenone and antimycin A, obtaining minimum oxygen consumption by the sample independent of mitochondrial respiration.

In the chamber test a linear regression expresses the dependence of the negative slope of the oxygen signal on  $c_{\text{O}_2}$ . The regression parameters have default values in the DatLab software of  $a^{\circ} = -2.0 \text{ pmol}\cdot\text{s}^{-1}\cdot\text{mL}^{-1}$  and  $b^{\circ} = 0.025$ , if no instrumental background test has been performed for calculating the experimental regression parameters. Using



these default values, the instrumental background oxygen consumption at air saturation (180  $\mu\text{M}$ ) and at 30  $\mu\text{M}$  are calculated at 2.5 and  $-1.3 \text{ pmol}\cdot\text{s}^{-1}\cdot\text{mL}^{-1}$  compared to 2.6 and  $-1.4 \text{ pmol}\cdot\text{s}^{-1}\cdot\text{mL}^{-1}$ , respectively, obtained on average in our background tests (Figure 7). At this level of agreement, it may be asked why and how frequently a user of the O2k should perform the chamber test. Regular testing provides IQC, ensuring that (1) the instrument is in an optimally functional state, (2) the operators have followed properly the SOP, and therefore (3) instrumental artifacts are excluded. In summary, instrumental QC is a cornerstone for experimental reproducibility.

Further analysis of  $\text{O}_2$  background parameters provides information on accuracy beyond reproducibility. Since oxygen diffusion is zero at air saturation, the instrumental background of  $2.6 \text{ pmol}\cdot\text{s}^{-1}\cdot\text{mL}^{-1}$  (Figure 7) is exclusively due to the  $\text{O}_2$  consumption by the POS. The  $\text{O}_2$  consumption by the POS, in turn, can be calculated from the electric current. The current or calibration signal R1-R0 was 2.04  $\mu\text{A}$  for the average sensor (Figure 3b). The flow of electrons of 1 A ( $= 1 \text{ C}\cdot\text{s}^{-1}$ ) is converted to the molar format (chemical units) by the Faraday constant  $F = 96\,485.33 \text{ C}\cdot\text{mol}^{-1}$ : the charge of 1 C is equal to the amount of 10.36  $\mu\text{mol}$  of electrons  $e^-$ . Division by the charge number of 4  $e^-/\text{O}_2$  converts this amount of  $e^-$  to 2.59  $\mu\text{mol}$  of  $\text{O}_2$  (Gnaiger 2020). Therefore, 2.04  $\mu\text{A}$  corresponds to an  $\text{O}_2$  consumption of  $2.04 \mu\text{C}\cdot\text{s}^{-1} \cdot 2.59 \mu\text{mol O}_2 = 5.29 \text{ pmol O}_2\cdot\text{s}^{-1}$ , equal to a theoretical volume-specific background  $\text{O}_2$  flux of  $2.64 \text{ pmol}\cdot\text{s}^{-1}\cdot\text{mL}^{-1}$  in a 2-mL chamber. Agreement between the  $\text{O}_2$  flux calculated from the signal of the POS and the  $\text{O}_2$  flux obtained experimentally confirms the accuracy of the measurement of  $\text{O}_2$  consumption by HRR.

## 5. Conclusions

Quality control in HRR is essential to minimize experimental errors and ensure reproducibility. Instrumental tests are standard operating procedures that provide internal quality control for the evaluation of instrumental performance, to assure both the functioning of the instrument and correct execution of the SOP by the operator before starting an experimental series. The present study presents a generally applicable procedure which can be implemented into an external QC management and interlaboratory ring tests. These SOPs represent key aspects of proficiency testing, for improving technical performance of laboratories and development of certified auditing for diagnostic applications.

### Abbreviations

BG	background	POS	polarographic oxygen sensor
$c_{\text{O}_2}$	oxygen concentration	PT	proficiency testing
HRR	high-resolution respirometry	QC	quality control
IQC	internal quality control	SD	standard deviation
$J^{\circ}_{\text{O}_2}$	instrumental background oxygen flux	SOP	standard operating procedure
$J_{\text{V},\text{O}_2}$	volume-specific oxygen flux	SUIT	substrate-uncoupler-inhibitor titration

## Acknowledgements

We thank Marco Di Marcello for technical support and performance of background experiments. This work was part of the Oroboros NextGen-O2k project, with funding from the European Union's Horizon 2020 research and innovation programme under grant agreement n° 859770.

## References

- Amaral OB, Neves K (2021) Reproducibility: expect less of the scientific paper. *Nature* 597:329-31. <https://doi.org/10.1038/d41586-021-02486-7>
- Brookman B, Mann I, eds (2021) *Eurachem guide: selection, use and interpretation of proficiency testing (PT) schemes* (3rd ed). Available from [www.eurachem.org](http://www.eurachem.org)
- Doerrier C, Garcia-Souza LF, Krumschnabel G, Wohlfarter Y, Mészáros AT, Gnaiger E (2018) High-Resolution FluoRespirometry and OXPHOS protocols for human cells, permeabilized fibers from small biopsies of muscle, and isolated mitochondria. *Methods Mol Biol* 1782:31-70. [https://doi.org/10.1007/978-1-4939-7831-1\\_3](https://doi.org/10.1007/978-1-4939-7831-1_3)
- Gnaiger E (2001) Bioenergetics at low oxygen: dependence of respiration and phosphorylation on oxygen and adenosine diphosphate supply. *Respir Physiol* 128:277-97.
- Gnaiger E (2008) Polarographic oxygen sensors, the oxygraph and high-resolution respirometry to assess mitochondrial function. In: *Mitochondrial dysfunction in drug-induced toxicity* (Dykens JA, Will Y, eds) John Wiley & Sons, Inc, Hoboken, NJ:327-52.
- Gnaiger E (2020) Mitochondrial pathways and respiratory control. An introduction to OXPHOS analysis. 5th ed. *Bioenerg Commun* 2020.2. <https://doi.org/10.26124/bec:2020-0002>
- Gnaiger E (2021) Bioenergetic cluster analysis – mitochondrial respiratory control in human fibroblasts. *MitoFit Preprints* 2021.8. <https://doi.org/10.26124/mitofit:2021-0008>
- Gnaiger E, Kuznetsov AV, Schneeberger S, Seiler R, Brandacher G, Steurer W, Margreiter R (2000) Mitochondria in the cold. In: *Life in the Cold* (Heldmaier G, Klingenspor M, eds) Springer, Berlin, Heidelberg:431-42. [https://doi.org/10.1007/978-3-662-04162-8\\_45](https://doi.org/10.1007/978-3-662-04162-8_45)
- Horan MP, Pichaud N, Ballard JWO (2012) Review: Quantifying mitochondrial dysfunction in complex diseases of aging. *J Gerontol A Biol Sci Med Sci* 67:1022-35. <https://doi.org/10.1093/gerona/glr263>
- Perry CG, Kane DA, Lanza IR, Neuffer PD (2013) Methods for assessing mitochondrial function in diabetes. *Diabetes* 62:1041-53. <https://doi.org/10.2337/db12-1219>
- Pesta D, Gnaiger E (2012) High-resolution respirometry. OXPHOS protocols for human cells and permeabilized fibers from small biopsies of human muscle. *Methods Mol Biol* 810:25-58. [https://doi.org/10.1007/978-1-61779-382-0\\_3](https://doi.org/10.1007/978-1-61779-382-0_3)
- Yépez VA, Kremer LS, Iuso A, Gusic M, Kopajtich R, Koňářková E, Nadel A, Wachutka L, Prokisch H, Gagneur J (2018) OCR-Stats: Robust estimation and statistical testing of mitochondrial respiration activities using Seahorse XF Analyzer. *PLOS ONE* 13:e0199938. <https://doi.org/10.1371/journal.pone.0199938>
- Zdrzilova L, Hansikova H, Gnaiger E (2022) Comparable respiratory activity in attached and suspended human fibroblasts. *PLoS ONE* 17:e0264496. <https://doi.org/10.1371/journal.pone.0264496>
- Zhang J, Nuebel E, Wisidagama DR, Setoguchi K, Hong JS, Van Horn CM, Imam SS, Vergnes L, Malone CS, Koehler CM, Teitell MA (2012) Measuring energy metabolism in cultured cells, including human pluripotent stem cells and differentiated cells. *Nat Protoc* 7: 1068-85. doi: 10.1038/nprot.2012.048

**Copyright:** © 2022 The authors. This is an Open Access preprint (not peer-reviewed) distributed under the terms of the Creative Commons Attribution License, which permits unrestricted use, distribution, and reproduction in any medium, provided the original authors and source are credited. © remains with the authors, who have granted MitoFit Preprints an Open Access publication license in perpetuity.



## Supplement

### S1. Variation of the slope of O<sub>2</sub> concentration $dc_{O_2}/dt$ at air saturation

R1 is measured in the open chamber, when the signal is expected to be constant at equilibrium with air. Maximal  $-dc_{O_2}/dt$  in mark R1 (Figure 2b; red plot) were 0.26 and 0.36  $\text{pmol}\cdot\text{s}^{-1}\cdot\text{mL}^{-1}$ , while the minima were -0.39 and -0.86  $\text{pmol}\cdot\text{s}^{-1}\cdot\text{mL}^{-1}$  in 2020 and 2021, respectively (Figure S1a). With a slight trend of increasing signal over time, the scatter indicated no persistence of drift of R1. Comparing these slopes in R1 with a maximum difference of 0.06  $\text{pmol}\cdot\text{s}^{-1}\cdot\text{mL}^{-1}$  between R1#1 and R1#2 (Figure 3a) suggests that the slopes in R1 were mainly due to short-term fluctuations of the oxygen signal.

The maximal absolute slope  $|dc_{O_2}/dt|$  for time intervals  $\Delta t$  of a few minutes (Figure S1a), few days (Figure 3a), and about one month (Figure 3b) decreased as  $\Delta t$  increased, averaging 0.6, 0.04 and 0.003 for a  $\Delta t$  of 4 to 15 min, 1 to 3 days and 27 to 35 days, respectively (Figure S1b). This suggests the lack of a persistent drift over time.

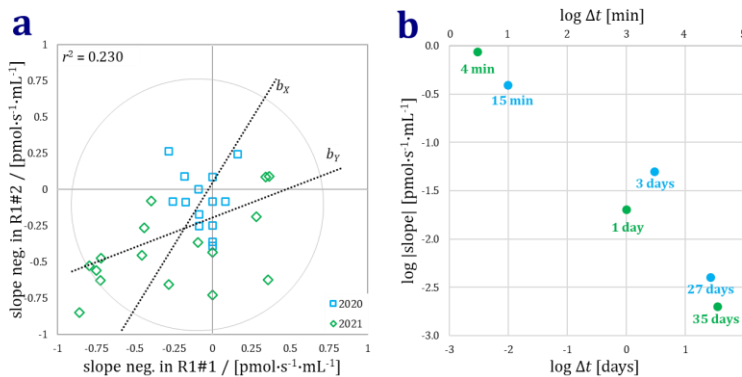


**Figure S1. Signal drift for O<sub>2</sub> concentration over time at air saturation. (a)** Negative  $c_{O_2}$  slope in marks R1 of 30 oxygen sensors measured in SOP-POS. R1#1 and R1#2 were 3 days (2020) or 1 day apart (2021). Horizontal and vertical lines: default intercept at 0/0. Dotted lines: ordinate  $b_y$  and abscissal  $b_x$

regression lines, with cross-over points  $X^* = -0.17 \text{ pmol}\cdot\text{s}^{-1}\cdot\text{mL}^{-1}$  and  $Y^* = -0.26 \text{ pmol}\cdot\text{s}^{-1}\cdot\text{mL}^{-1}$ , compared to the medians of -0.09 and -0.25  $\text{pmol}\cdot\text{s}^{-1}\cdot\text{mL}^{-1}$ . The circle, centered at the cross-over point, indicates the lack of correlation with circular data distribution. Data points are within  $\pm 1 \text{ pmol}\cdot\text{s}^{-1}\cdot\text{mL}^{-1}$ . **(b)** Maximal  $|dc_{O_2}/dt|$  (2020: blue dots; 2021: green dots) as a function of time intervals  $\Delta t$  from 4 minutes to 35 days.

### S2. MiPNet links

MiPNet06.03 (2022) O2k Quality Control 1: Polarographic oxygen sensors and accuracy of calibration. Mitochondr Physiol Network 06.03(20):1-8.

- [https://wiki.oroboros.at/index.php/MiPNet06.03\\_POS-calibration-SOP](https://wiki.oroboros.at/index.php/MiPNet06.03_POS-calibration-SOP)

MiPNet14.06 (2020) O2k Quality Control 2: Instrumental oxygen background correction and accuracy of oxygen flux. Mitochondr Physiol Network 14.6(08):1-16.

- [https://wiki.oroboros.at/index.php/MiPNet14.06\\_Instrumental\\_O2\\_background](https://wiki.oroboros.at/index.php/MiPNet14.06_Instrumental_O2_background)

MiPNet18.10 (2019) O2k-specifications for respirometry and comprehensive OXPHOS analysis. Mitochondr Physiol Network 18.10(09):1-8.

- [https://wiki.oroboros.at/index.php/MiPNet18.10\\_O2k-Specifications](https://wiki.oroboros.at/index.php/MiPNet18.10_O2k-Specifications)

MiPNet19.18B (2021) Service of the polarographic oxygen sensor OroboPOS. Mitochondr Physiol Network 19.18(B09):1-7.

- [https://wiki.oroboros.at/index.php/MiPNet19.18B\\_POS-service](https://wiki.oroboros.at/index.php/MiPNet19.18B_POS-service)